SBRHI-99-1

Light Fragment Yields from Au + Au Collisions at 11.5 A GeV/c

J. Barrette[5], R. Bellwied[9], S. Bennett[9], R. Bersch[7], P. Braun-Munzinger[2], W. C. Chang[7], W. E. Cleland[6], M. Clemen[6], J.D. Cole[4], T. M. Cormier[9], Y. Dai[5], G. David[1], J. Dee[7], O. Dietzsch[8], M.W. Drigert[4], K. Filimonov[5], J. R. Hall[9], T. K. Hemmick[7], N. Herrmann[2], B. Hong[2], C. L. Jiang[7], S.C. Johnson[7], Y. Kwon[7], R. Lacasse[5], D. Miskowiec[2], Q. Li[9], T. W. Ludlam[1], S. McCorkle[1], S. K. Mark[5], R. Matheus[9], E. O'Brien[1], S. Panitkin[7], T. Piazza[7], M. Pollack[7], C. Pruneau[9], Y. J. Qi[5], M. N. Rao[7], E. L. Reber[4], M. Rosati[5], N. C. daSilva[8], S. Sedykh[7], J. Sheen[9], U. Sonnadara[6], J. Stachel[3], H. Takai[1], E. M. Takagui[8], S. Voloshin[6], T. Vongpaseuth[7], J. P. Wessels[3], C. L. Woody[1], N. Xu[7], Y. Zhang[7], Z. Zhang[6], C. Zou[7]

(E877 Collaboration)

[1] *Brookhaven National Laboratory, Upton, NY 11973*

[2] *Gesellschaft für Schwerionenforschung, Darmstadt, Germany*

[3] *Physikalisles Institut, Universität Heidelberg, Heidelberg, Germany*

[4] *Idaho National Engineering Laboratory, Idaho Falls, ID 83415*

[5] *McGill University, Montreal, Canada*

[6] *University of Pittsburgh, Pittsburgh, PA 15260*

[7] *The University at Stony Brook, Stony Brook, NY 11794*

[8] *University of São Paulo, Brazil*

[9] *Wayne State University, Detroit, MI 48202*

Abstract

Inclusive double differential multiplicities of deuterons, ^{3}H, ^{3}He, and ^{4}He measured by E877 for 11.5 A GeV/c Au+Au collisions at the AGS are presented. Light fragments at beam-rapidity are measured for the first time at AGS energies. Beam rapidity deuterons and ^{4}He yields and transverse slopes are strongly dependent on impact parameter and the shape of deuteron spectra is not consistent with that expected from a simple thermal distribution. The deuteron yields relative to protons are analyzed in terms of a simple coalescence model. While results are consistent with an increase in source size compared to lighter collision systems at the same energy, they are inconsistent with a simple coalescence model due to a rapidity dependence of the coalescence parameter B_d. A novel technique utilizing a simple source and a coalescence code is developed for studying deuteron formation in heavy-ion collisions. The strong dependence of deuteron yields on collective motion implies that deuteron yields relative to that of protons can be used as a tight constraint on source parameters. Sample calculations using measured protons and deuterons at the AGS are shown to significantly constrain source properties.

Typeset using REVTEX

INTRODUCTION

The study of heavy-ion collisions at ultra-relativistic energies has been pursued with the intent of observing matter at extreme temperatures and densities, the eventual goal being the production and study of deconfined and/or chirally restored matter. Although the relativistic heavy-ion program has developed over a number of years, and various hadronic observables have been studied, a complete characterization of the state formed during the high density phase of the collision is still outstanding.

Measurements of light fragments in the participant region of heavy-ion collisions are of interest since model calculations can be used to deduce measures of the source volume from the yield of deuterons relative to that of protons [1–5]. The yield of light fragments is analagous to the two particle correlation between nucleons by final state interactions [4] and this can be incorporated into a theoretical framework which deduces the density of the interaction region at freeze-out.

In this publication we will report on investigations of the characteristics of light nuclei spectra utilizing the E877 spectrometer, located at Brookhaven National Laboratory's (BNL) Alternating Gradient Synchroton (AGS). Spectra and yields of light nuclei, including deuterons, ^{3}H, ^{3}He, and ^{4}He will be presented and compared to similar measurements at other beam energies and for various colliding systems.

EXPERIMENTAL APPARATUS

The E877 apparatus has already been described in [5]. Global observables, single particle spectra of protons, pions [6] and kaons [7,8] and two particle correlations [9–11] as well as collective flow [12] have been studied by E877 at the AGS due to its unique experimental configuration at these energies. The experiment primarily consists of three components: (1) a set of scintillators and silicon detectors for beam definition; (2) a near 4π calorimetry coverage and a large acceptance charged particle multiplicity measurement, providing global event properties; and (3) a forward spectrometer, allowing measurements of charged particles. Figure 1 provides a schematic diagram of the E877 experimental setup for the 1994 run. The z direction was defined to be along the beam and the y axis was defined to be out of the page (vertical).

The data presented here were collected in the fall of 1994. After event selection cuts are applied approximately $5.4 \cdot 10^6$ events of the 4% most central collisions were available for analysis.

Beam Definition

In order to verify the beam composition, determine its momentum and direction, and provide the start time of the experiment a number of detectors were placed upstream of the target.

A series of four plastic scintillators (S1, S2, S3, S4) were used for the time reference definition in the experiment. Scintillators S1 and S3 were ring-shaped veto detectors while scintillators S2 and S4 were ellipsoidal detectors placed at 45° relative to the beam. Fast rise time phototubes were utilized on S2 and S4 providing the interaction time with a typical Gaussian standard deviation of $\sigma = 35 - 40$ ps.

Two silicon microstrip detectors (BVER's) measured the beam angle in the xz-plane and were located between S2 and S4. The detectors were 300 μm thick and composed of 320 strips with a 50 μm pitch. This provided a measurement of the beam angle with a resolution of ~ 40 μrad and determined the x coordinate of the beam at the target to 300 μm [13]. The BVER's were also used to tag those events in which two or more particles traversed the experiment within the same 1 μs bin.

To eliminate beam components with incorrect nuclear charge number, a silicon semiconductor counter (SILI) was placed 2.5 cm upstream of the target to measure the energy loss of the beam.

Event Characterization

For one central Au + Au event, the number of produced pions and nucleons of each isospin state is approximately 150. Two large, highly segmented calorimeters were used to quantify the centrality and reaction plane of the collisions. Together these detectors cover nearly 4π in the center-of-mass frame.

The Target Calorimeter (TCAL) [14,15] consists of 832 NaI(Tl) crystals surrounding the target with a polar angle coverage of $48^\circ < \theta < 135^\circ$ ($-0.5 < \eta < 0.8$). Each crystal has a depth of 13.8 cm, or about 5.4 radiation lengths (0.34 hadronic interaction lengths).

The Participant Calorimeter (PCAL) is a finely segmented lead/iron/scintillator calorimeter consisting of 16 azimuthal, 8 radial, and 4 depth sections. It covers a polar angle region of $1^\circ < \theta < 47^\circ$ ($0.83 < \eta < 4.7$). There is a small opening in the PCAL ($-136 < \theta_x < 16$ mrad; $-11 < \theta_y < 11$ mrad) with iron wedges along the inside which define the acceptance of the forward spectrometer.

Forward Spectrometer

For measuring the momentum and time-of-flight of all charged particles accepted into the forward region, two vertex chambers, two drift chambers and two time of flight hodoscope walls have been constructed. These detectors are also shown schematically in Fig. 1.

A set of wire chambers with a highly segmented cathode pad readout are placed 2 m from the interaction region separated from each other by 25cm (VTXA and VTXB). These chambers were implemented for the 1994 Au+Au run [16] in order to aid in recognizing secondary vertices. Each chamber has a cathode pad plane segmented into 508 read out channels providing a position resolution of 100 μm horizontally and 1.44 mm vertically, resulting in a vertex resolution in x of $1.71/\tan\theta$ mm; they were not used in this analysis.

The analyzing magnet, situated after the vertex chambers, could be run in two polarities in order to study possible systematic errors in momentum with the forward spectrometer and to optimize the acceptance for positive and negative particles. The produced magnetic field was $3,353$ Gauss in the y direction with a length of 100 cm in z and a polarity which bent positive particles in the negative x direction.

Two drift chambers (DC2 and DC3) provided x and y information of the tracks and were used to determine the rigidity of each track; each drift chamber was composed of six planes of wires which measured the position in the bending plane of the magnet, *i.e.* the xz-plane, with a resolution of 250 μm (300 μm) for DC2 (DC3). Furthermore, DC2 and DC3 contained cathode pad planes segmented into a series of chevron-shaped pads with anode wires parallel to the y direction; this provides y measurements of charged particles with a resolution of typically a few percent of the pad size. Each drift chamber had two segmentation size regions, resulting in y-resolutions of 2.3 mm (15 mm) in DC2 and 4.3 mm (36 mm) in DC3 depending on the pad size.

The MWPCs were a series of multi-wire proportional chambers with vertical anode wires spaced 5.08 mm apart. They were used for track confirmation in the high multiplicity environment of Au+Au collisions.

The TOFU [17] was an array of 160 plastic scintillators aligned vertically and placed behind DC3; it provided a resolution of $85-100$ ps in time-of-flight measurements and a 1 cm vertical position resolution. The FSCI was a second hodoscope which also measured the time-of-flight at a distance of 31 m from the target with a resolution of 350 ps. It was utilized in this analysis only as a study of TOFU systematics.

A CsI photon detector, located 35 m from the target for measurement of photons from the collision, and a uranium calorimeter (UCAL) behind it, which provided neutron rejection and a measurement of forward energy, were not utilized in this analysis.

DATA ANALYSIS

Particle rigidity was determined from the radius of curvature of the track (R) through the magnet and the value of the magnetic field B:

$$\frac{\text{rigidity}}{e} = \frac{\sqrt{{p_x}^2 + {p_z}^2}}{Ze} = RB \tag{1}$$

where Ze is the charge of the particle. The vertical momentum component, p_y, is calculated from the vertical position of the track at the TOFU. The reconstructed mass of each particle is then given by

$$m^2c^4 = \frac{p^2c^2}{\beta^2\gamma^2} \tag{2}$$

where β and γ are calculated from the time-of-flight measurement coupled with the path length to the TOFU slat.

The charge of each particle is determined from the energy deposition in the TOFU slat. Shown in Fig. 2 is the distribution of pulse-heights for those particles corresponding to the deuteron mass peak at beam rapidity. A clear $Z = 1$ peak is visible as well as a $Z = 2 \cdot 1$, corresponding to two $Z = 1$ tracks striking the same TOFU slat, as well as a $Z = 2$ peak corresponding, in this case, to ^{4}He. The resulting distribution is fit to three Landau functions with a non-linear response due to the saturation of the photomultiplier tubes associated with the TOFU. The standard E877 analysis cut on the TOFU pulse-height distribution at 1.4 corresponds to a $\approx 10\%$ loss in the $Z = 1$ yield with no contamination from $Z = 2$.

Deuterons

Since $\delta m/m \propto \delta p/p$ and momentum measures worsen at larger values, mass measurements at large momenta yield poor resolution. At momenta near beam rapidity, for example, deuteron selection is complicated by the tail of the proton peak. To account for this effect, a systematic background subtraction technique was developed [18]. Shown in Fig. 3 is the reconstructed distribution of mass-squared in several $p_t = \sqrt{({p_x}^2 + {p_y}^2}$ and $y_{deut} = 0.5 \ln(E + p_z/E - p_z)$ bins. At low momentum, the deuteron and proton peaks are clearly distinguishable from the proton distribution. In this region of phase space, the mass-squared distribution is fit to two Gaussians and either an exponential or linear background[1]. At higher momenta, the proton and deuteron mass-squared distributions broaden, due to the momentum resolution of the apparatus, and the background is negligible. In this region of phase-space, shown Fig. 3B, the mass-squared distribution is fit to two Gaussian distributions. In the $2.6 < y < 3.0$ region, the momentum resolution smearing coupled with the approximately equal particle yields for protons and deuterons, causes the peaks to overlap (Fig. 3C), resulting in a loss of seperation of deuterons from protons in this region. However, at deuteron rapidity $y > 3.0$ the contamination of protons is minimal because the proton would need to be traveling at twice the beam momentum. Thus, a deuteron peak is again visible (Figure 3D) and the yield can be determined by fitting this region to a single Gaussian.

The yield of deuterons (N_d) in each small bin of phase space is determined from the parameters of a Gaussian fit to the deuteron peak:

$$N_d = \sigma_d A_d \sqrt{2\pi}/\Delta m^2 \tag{3}$$

where ${\sigma_d}^2$ and A_d are the variance and amplitude of the Gaussian distribution fit to the deuteron peak, and Δm^2 is the bin width. Those regions of momentum space that fall between the first two regions outlined above, Figure 3A and B, respectively, have been fit to both functions in order to determine the systematic error due to the choice of fit funcion. The resulting yield of deuterons agree within 5% between both fits.

Tritons

The triton signal is complicated by the fact that its mass-squared distribution is wider than the deuteron's due to multiple scattering and its yield is 1-2 orders of magnitude lower

[1]The systematic error associated with the choice of the background function has been found to be less than 5% [18]

than that of the deuteron due to multiple scattering effects. However, a technique similar to that used for the deuterons can also be utilized to measure the yield of tritons in the collisions studied here. In Fig. 4 is shown the reconstructed mass-squared distribution in various y_{trit} bins for $p_t < 0.5$ GeV/c. A clear triton peak is visible to the right of the deuteron peak. The yield of tritons was calculated for each rapidity and p_t bin by fitting this distribution to a Gaussian at the mass of the triton with an exponential background from the deuteron tail; the choice of an exponential or Gaussian background was found to have less than a 5% effect on the resulting yields. Several examples of these fits are shown in Fig. 4.

Helium Isotopes

Helium isotopes can be seperated from $Z = 1$ species by cutting on energy deposition in the scintillators as described earlier. The ^{3}He signal is found by recalculating the mass-squared according to eqn. 2 assuming $Z = 2$. This will cause all $Z = 1$ particles which pass the scintillator pulse-height cut to be found at double their actual mass. The ^{3}He peak in this case is found between, and clearly differentiated from, the proton and deuteron residual peaks, respectively located at $m^2 \approx 4$ and $m^2 \approx 13$ GeV/c, as shown in Fig. 5. In this case, the peak is located under the proton tail above $y \sim 2.0$ and the yield of ^{3}He in each bin may be extracted by fitting the mass-squared distribution to two Gaussians corresponding to the ^{3}He and proton peaks.

So far the determination of particle specie yield was determined by cutting on the energy loss in the TOFU and, subsequently, fitting the peak in the m^2/Z^2 spectrum. This method can not be applied to ^{4}He because the ^{4}He peak in m^2/Z^2 space is buried under the significantly larger deuteron peak. We therefore use an orthogonal approach to identify ^{4}He [18]: we cut on the m^2/Z^2 peak and fit the $Z = 2$ peak in the TOFU pulse height distribution. As described earlier, this distribution has two peaks, corresponding to $Z = 1$ and two $Z = 1$ particles, at all but beam rapidity where an additional $Z = 2$ peak is evident as shown in

Fig. 2. These peaks are fit, at beam rapidity for $p_t < 2$ GeV/c, to a Landau distribution and the yield is then determined from the integral under the fit to the $Z = 2$ distribution. The overall systematic error for this peak extraction procedure has been found to be less than 10% [18].

RESULTS

Mid-rapidity

Shown in Fig. 6 are deuteron invariant multiplicities as a function of p_t and y. The data have bin widths of 20 MeV in p_t and 0.1 in y. The invariant multiplicity is flat as a function of p_t and y over the entire measured range and is thereby indescribable by a finite inverse slope parameter near mid-rapidity ($y_{mid} \approx 1.6$).

In Fig. 7 are shown the measured invariant multiplicities of ^{3}H and ^{3}He for the 4% most central collisions. The spectra are presented as a function of rapidity for two p_t regions. The error bars only reflect the uncertainty in the fitted function and do not include the systematic errors, estimated to be $\sim 20\%$ for both ^{3}He ^{3}H, dominated by the uncertainty in the assumed background fit function [18].

Beam-rapidity

In Fig. 8 are shown invariant multiplicities for deuterons at beam rapidity for the 4% and 10-20% most central events. As noted above, deuterons at beam rapidity are easily extracted from the mass-squared distribution. Beam rapidity distributions have a finite slope parameter. The 4% central beam rapidity deuterons are distinctly harder (larger inverse slope parameter) than deuterons from the lower centrality collisions. Over the range in p_t in which we measure, a fit to a Boltzmann gives $T_B = 49.6 \pm 1.4$ MeV and $T_B = 83 \pm 2$ MeV for the 4% and 10-20% centrality bins, respectively. However, the reduced χ^2 of each of these fits is greater than 4, implying a Boltzmann shape does not describe the measured distribution.

In Fig. 9 are shown ^{4}He measurements at beam rapidity for the 4% and the 10-20% centrality range. In the lower centrality range, the ^{4}He yield is a factor of 10 higher than for the higher centrality, indicating that beam rapidity ^{4}He are primarily produced by spectator fragmentation.

COMPARISONS

Light fragments from heavy-ion collisions have historically been studied via a coalescence model [2,19] which assumes deuteron formation takes place at freeze-out. Since the binding energy of the deuteron is 2.24 MeV, it is easily broken apart in the fireball region where current models estimate the temperature to be 120-170 MeV [20,21]. In the coalescence formulation [19] the probability of forming a deuteron is greatest when a proton and neutron at freeze-out have a small relative momentum such that [23]

$$P_d(\vec{v} = \vec{v_d}) \propto P_p(\vec{v_p} = \vec{v_d}) \cdot P_n(\vec{v_n} = \vec{v_d}) \tag{4}$$

where $P(\vec{v})$ is the probability of a particle having a velocity $\vec{v}$ close enough in phase space for coalescence. Assuming that the proton and neutron distributions are similar, the deuteron momentum distribution is then given by

$$E_d \frac{d^3 N_d}{dp^3}(p_d) = B_d \left(E_p \frac{d^3 N_p}{dp^3}(p_p) \right)^2 \tag{5}$$

where $p_d = 2p_p$ which can be easily generalized to heavier fragments as

$$E_A \frac{d^3 N_A}{dp^3}(p_A) = B_A \left(E_p \frac{d^3 N_p}{dp^3}(p_p) \right)^A \tag{6}$$

where $p_A = Ap_p$. In eqns. 5 and 6, B_A is a phenomenological parameter known as the coalescence constant. In proton-nucleus collisions B_A has been related to the interplay between the binding energy of the deuteron and the optical potential of the target nucleus [19]. For nucleus-nucleus collisions it was recognized that the idea of a nuclear optical potential was no longer meaningful and Schwarzschild and Zupančič [2] expressed the coalescence parameter in terms of a momentum radius p_0 within which a proton and neutron would coalesce to form a deuteron. More generally, for the case of a source of Z protons and N neutrons with mass number of the cluster A

$$B_A = \left(\frac{2s_A+1}{2^A}\right) \frac{{R_{np}}^N}{N!Z!} \left(\frac{4\pi}{3}{p_0}^3\right)^{A-1} \tag{7}$$

where s_A is the spin of the cluster and R_{np} is the neutron to proton ratio in the source. Therefore, the coalescence parameter in these models is simply related to the momentum difference between corresponding protons and neutrons and is described by a simple step function in the coalescence probability at p_0. Note that no dependence on the colliding system exists in this model which described deuteron and ^{3}H/^{3}He production very well in nucleus-nucleus reactions at Bevalac [23,24] energies (about $0.1 - 2$GeV$\cdot$A) and in p-nucleus collisions, at FNAL [25] energies. For all of these energies, only a single B_A was needed to describe the light fragment distributions from the proton spectra. However, for nucleus-nucleus collisions at AGS energies and above a dramatic drop in the coalescence parameter and a strong dependence on the centrality of the collision [5,26] was observed. For higher beam energies, when nuclear collisions produce a large number of secondary particles, B_d was no longer independent of beam energy or composition due to the fact that the source decoupled at a size larger than the mean size of a deuteron, $R_{rms} = 2.1$ fm [1,3,27]. In this case, B_d was deduced to be inversely proportional to the volume of the source at freeze-out [1,28]. In the model of Sato and Yazaki, for example,

$$B_d = \frac{3}{4}\frac{(8\pi)^{3/2}}{Z!N!}\left[\frac{\nu_d \nu}{(\nu_d+\nu)}\right]^{3/2} \tag{8}$$

here $\nu_d = .20fm^{-2}$ is the Gaussian wave function parameter for a deuteron and ν is directly related to the nucleon freeze-out radius by

$$R_{rms} = (3/2\nu)^{1/2}. \tag{9}$$

Other models [3] also utilize a wave-function description and a density matrix formalism to describe deuteron formation. Many of the models are similar though, with the exception of large cascade codes [27,29], none of them account for collective expansion. Further, though there have been some attempts at a fully relativistic treatment [30], the generalization to relativity is non-trivial because of difficulties in the proper relativistic treatment of bound states [3].

Coalescence Parameter B_d

To properly calculate B_d for our data set, the contamination of protons from Λ decays must be subtracted from the measured proton spectra. This was studied in [18] utilizing the measured Λ yield in Au+Au collisions [31] and knowledge of the acceptance and reconstruction efficiency of the experimental apparatus. Over the measured acceptance region, the hyperon contamination to the proton spectra was found to be no more than 10%.

After correcting for hyperon contamination, B_d can be calculated as a function of p_t and y. We note that, within the acceptance of the present measurement, no variance of B_d as a function of p_t. However, there is a noticeable rapidity dependence of B_d as shown in Fig. 10. If B_d is related to volume at freeze-out, such a result may imply a changing effective freeze-out volume as a function of rapidity. Similar dependencies of B_d on p_t at Bevalac energies have also been noted [24].

Shown in Fig. 11 is a collection of data from Bevalac [23,24] energies as well as AGS measurements in Si + Al [5], Si + Pb [32] and Au + Au collisions from this data sample. The error on the Au+Au data point corresponds to the range of B_d measures shown in Fig. 10. All presently measured values of B_d for central Au+Au collisions are significantly lower than the Si+Al or Si+Pb data points, consistent with the theory that B_d corresponds to the volume at freeze-out as well as consistent with the increased source size according to two-proton correlations also measured by E877 [10].

Note that the coalescence parameter measured in these Au+Au collisions is approximately one-tenth of that measured at Bevalac energies, implying in the models of [1,28] that the volume at feeze-out in AGS Au+Au collisions is ten times that at Bevalac energies; indeed, the rms radius deduced from eqn. 9 is $R_{rms} \approx 12$ fm. Such a deduction is inconsistent with two particle correlations measured at the AGS [9–11].

A possible reason for such an inconsistency is that the models which deduce an inverse volume dependence [1,28] do not account for collective motions in the source. As has been shown by [33], the yield of deuterons is highly dependent on the amount of collective motion in the source. Hence, B_d is not simply related to the volume but also the position-momentum correlations at freeze-out. If the source is perfectly correlated, then proton neutron paris that freeze-out near one another in space will have very similar momentum vectors. The deuteron yield would be larger in this case than for a random source. As such, any consistent model of deuteron production must account for correlations in the source.

Therefore, in order to completely describe deuteron production, a more sophisticated model of the source that includes dynamical correlations must be incorporated. In large cascade codes it is difficult to easily vary source parameters. This leads us to choose a simpler model.

A SOLUTION

An analytic, hydrodynamically motivated model, devised by S. Chapman, J.R. Nix, and U. Heinz [34] has been implemented to describe the source in a heavy ion collisions [35]. This model uses an emission function (S) for a finite expanding thermalized source where

$$E_K \frac{d^3N}{d^3K} = \int d^4x S(x,K). \tag{10}$$

The source includes longitudinal and transverse collective motion with an underlying temperature, given by

$$S(x,K) = \frac{M_t \cosh(\eta - Y)}{(2\pi)^{7/2}\Delta\tau} exp\left[-\frac{K \cdot u(x)}{T} - \frac{(\tau-\tau_0)^2}{2(\Delta\tau)^2} - \frac{r^2}{2R^2} - \frac{(\eta-\eta_0)^2}{2(\Delta\eta)^2}\right] \tag{11}$$

where

$$\eta = \frac{1}{2} ln[(t+z)/(t-z)]$$

$$
\begin{aligned}
\tau &= \sqrt{(t^2 - z^2)} \\
Y &= \frac{1}{2} ln[(1+\beta_l)/(1-\beta_l)] \\
K \cdot u(x) &= M_t \cosh(\eta - Y)\cosh\eta_t(r) - K_t \frac{x}{r}\sinh\eta_t(r) \\
\eta_t(r) &= \eta_f(r/R).
\end{aligned}
$$

In this model (x, y, z, t) is the freeze-out position four vector, $r = \sqrt{x^2 + y^2}$ and β_l and M_t are the longitudinal velocity and transverse mass, respectively. Furthermore, $\Delta\tau$, $\Delta\eta$ and R describe the respective Gaussian widths of the proper time, longitudinal velocity and one dimensional Gaussian radius.

For the determination of deuteron yields, a program devised by R. Mattiello [33,37] was implemented. It utilizes a method applied to bombarding energies from 1 GeV per nucleon in conjunction with the intranuclear cascade model and QMD [38] to AGS and SPS energies with the cascade models RQMD [33,37] and ARC [29]. In this model, the number of deuterons is given by a summation over all proton and neutron pairs (i_n, j_p) at freeze-out

$$
dN_d = \frac{3}{8}\left\langle \sum_{i_n, j_p} {\rho_d}^W(\mathbf{\Delta x}, \mathbf{\Delta y}) \right\rangle d^3(p_{i_n} + p_{j_p}) \tag{12}
$$

where ${\rho_d}^W$ is the Wigner density of the Hulthén deuteron wave function and the value of 3/8 derives from spin (3/4) and isospin (1/2) considerations assuming no dynamical correlations in these sectors [27]. Therefore, by projecting the neutron/proton position-momentum distribution on the deuteron wave-function via this Wigner method, we may determine the distribution of deuterons in phase-space given any particular source of nucleons.

Shown in Fig. 12 is the distribution of the reduced χ^2 minus the minimum χ^2 with respect to the measured deuterons calculated as a function of T and R with a resolution of 10 MeV and .25 fm respectively. For this study we assume that τ_0 = 3fm and $\Delta\tau$ = 1fm in Eqn. 11. [2] The technique we utilize for mapping out this χ^2 space is the following: For each value of temperature T and one dimensional Gaussian radius R, the transverse and

[2]For SPS energies, Wiedemann, Tomasik and Heinz [35] found $\Delta\tau \sim 1.5$ fm/c from two particle

longitudinal proton spectra uniquely define the transverse (η_f) and longitudinal ($\Delta\eta$) boost velocities. Every value of T and R in Fig. 12 can describe the proton transverse spectra given a particular η_f at mid-rapidity.

However, we have found that the proton rapidity distribution in this model poorly reproduces the longitudinal data [6,39], with a reduced χ^2 on the order of 10 for all choices of T, R and $\Delta\eta$. Furthermore, the shape of the transverse nucleon distribution in this model is assumed to be constant as a function of rapidity, in conflict with experimental measures [6]. The assumptions inherent in the model [34] regarding a hydrodynamical source are not valid for nucleons at AGS energies. Due to the lack of another analytic model which could be used, we implement this model in the region of mid-rapidity, by fitting η_f to the proton p_t distribution at mid-rapidity and $\Delta\eta$ to the rapidity distribution with the caveats described above. The inherent problems of this source in describing nucleons at AGS energies do not detract from the conclusion of the analysis, that deuterons are a sensitive constraint on source parameters.

For this analysis, the proton spectra from E866 Au+Au collisions [39] are utilized due to their coverage of protons at mid-rapidity. The model is therefore fit with these two parameters to the proton spectra. After the proton distribution is determined, the deuteron yields at mid-rapidity are calculated with the coalescence afterburner described above. Results are compared to deuterons measured by E877 at mid-rapidity and $p_t < 0.6$ GeV/c.

From this simple study, we note that the deuterons are strongly dependent on the parameters in our analytic source that describe the source of nucleons. As a result, they can be utilized to significantly restrict theoretical models. By this method, deuterons, similar to other correlation measurements and single particle spectra, are a combined measure of both size and collective motion.

---

correlations while Scheibl and Heinz [36] noted that $\tau_0 \sim 9$fm/c. Similar numbers for AGS energies have not been published.

Note, however, that this method has not constrained $\Delta\tau$ or τ_0. Varying these attributes from the values chosen above by a factor of two can vary the yield of deuterons by 10%. As a result, deuterons cannot be used exclusively to define the nucleon source of a heavy-ion collision and, instead, measures of several observables are needed to further restrict the allowable regions of phase space.

Finally, note that T and R determined in Fig. 12 denote only the *nucleon* temperature and radius with no assumption of intraspecies equilibration as is present when combining nucleon and meson measures.

CONCLUSIONS

We have measured light fragment yields at both mid and beam rapidities. Invariant multiplicities have been presented for deuterons, ^{3}H, and ^{3}He at mid-rapidity. Deuterons at mid-rapidity have been interpreted in a coalescence framework. The resulting coalescence parameter (B_d) is consistent with an increase in source size from collisions of lighter nuclei at the same energy. However, a clear dependence on rapidity of B_d points to a break-down in the simple assumptions of this model.

We have shown that deuterons can be used as a sensitive constraint on source parameters in a heavy ion collision by incorporating a simple, hydrodynamically motivated nucleon source function coupled with a coalescence algorithm. The results show that deuterons are a convolution of volume and collective effects, similar to other correlations measurements. These results can be used in conjunction with other measure of the source to tightly constrain theoretical models and assumptions.

First measurements of beam rapidity deuterons and ^{4}He at AGS energies have also been made. The resulting distributions have a strong centrality dependence, consistent with a production mechanism dominated by spectator fragmentation.

ACKNOWLEDGEMENTS

We would like to thank the BNL AGS and tandem operations staff and Dr. H. Brown for providing the beam. This work was supported in part by the U.S. DoE, the NSF, the NSERC, Canada and CNPq, Brazil.

We are grateful to Dr. Raffaele Mattiello, who provided the coalescence code utilized in this study and to Drs. J. H. Lee and C. Chasman for providing us with the measured E866 protons.

REFERENCES

[1] H. Sato and K. Yazaki, Phys. Lett. **98B** (1981) 153.

[2] A. Schwarzschild and Č. Zupančič, Phys. Rev. **129** (1963) 854.

[3] S. Mrówczyński, J. Phys. **G13** (1987) 1089.

[4] S. Mrówczyński, Phys. Lett **B 277** (1992) 43.

[5] J. Barrette *et al.* (E877 Collaboration), Phys. Rev. **C50** (1994) 3047; Phys. Rev. **C50** (1994) 1077

[6] J. Barrette *et al.* (E877 Collaboration), in progress; T. Piazza, PhD thesis, SUNY at Stony Brook (1997); R. Lacasse, PhD thesis, McGill University (1997)

[7] M. Pollack, PhD thesis, SUNY at Stony Brook (1997).

[8] J.P. Wessels for the E877 Collaboration; Nucl. Phys. **A638** (1998) 69c.

[9] J. Barrette *et al.* (E877 Collaboration), Phys. Rev. Lett. **78** (1997) 2916.

[10] J. Barette *et al.* (E877 Collaboration), in progress; S. Panitkin, PhD thesis, SUNY Stony Brook (1997)

[11] T. Vongpaseuth for the E877 Collaboration, RHIP '97 Proceedings, Czechoslovak J. of Phys. **48** (1998) Suppl. S1; T. Vongpaseuth, PhD thesis, SUNY Stony Brook (1999).

[12] J. Barrette *et al.*, (E877 Collaboration) Phys Rev. **C55** (1997) 1420; J. Barrette *et al.* Phys. Rev. **C59** (1999) 884.

[13] J. Dee, PhD thesis, SUNY at Stony Brook (1995).

[14] L. S. Waters, PhD thesis, SUNY at Stony Brook (1990).

[15] J. Barrette *et al.* (E877 Collaboration) Phys. Rev. Lett **70** (1993) 2996.

[16] R. Bersch, MSI thesis, SUNY at Stony Brook (1995).

[17] R. Lacasse *et al.*, Nucl. Instr. Meth. **A408** (1998) 408.

[18] S.C. Johnson, PhD thesis, SUNY at Stony Brook (1997).

[19] S. T. Butler and C. A. Pearson, Phys. Rev. **129** (1963) 836.

[20] P. Braun-Munzinger, J. Stachel, J.P. Wessels, Nu Xu Phys. Lett. **B344** (1995) 43; Phys. Lett. **B365** (1996) 1.

[21] E. Schnedermann, J. Sollfrank, U. Heinz Phys. Rev. C **48** (1993) 2462.

[22] U. Heinz, nucl-th/9810056; talk given at Strange Quark Matter '98, Padova, Italy; to be published in J. Phys. G

[23] S. Nagamiya *et al.*, Phys. Rev. C **24** (1981) 971; Lemaire *et al.*, Phys. Rev. Lett. **37**, (1976) 667; R. L. Auble *et al.*, Phys. Rev. C **28** (1983) 1552.

[24] S. Wang *et al.*, Phys. Rev. Lett. **74** (1995) 2648.

[25] J. W. Cronin *et al.*, Phys. Rev. D **11** (1975) 3105.

[26] J. Simon-Gillo for the NA44 collaboration, Nucl. Phys. **A590** (1995) 483c; S. Kabana for the NA52 collaboration, Nucl.Phys **A638** (1998) 411c.

[27] J.L. Nagle, B.S. Kumar, D. Kusnezov, H. Sorge, and R. Mattiello, Phys. Rev. C **53** (1996) 367.

[28] A.Z. Mekjian, Phys. Rev. C **17** (1978) 1051; Nucl. Phys. **A312** (1978) 491.

[29] D. E. Kahana *et al.*, Phys. Rev. C **54** (1996) 338.

[30] C. B. Dover, Phys. Rev. C **44**(1991) 1636.

[31] S. Ahmad *et al.* (E895 Collaboration), Phys. Lett. **B382** (1996) 35.

[32] T. Abbott *et al.* (E802 Collaboration), Phys. Rev. C **50** (1994) 1024.

[33] R. Mattiello, A. Jens, H. Sorge, H. Stöcker, W. Greiner, Phys. Rev. Lett **74** (1995)

2180.

[34] S. Chapman, J.R. Nix, and U. Heinz, Phys. Rev. C **52** (1995) 2694.

[35] U.A. Wiedemann, B. Tomasik, U. Heinz, Nucl. Phys. **A638** (1998) 475c; B. Tomasik, U. Heinz, U.A. Widemann, Y.-F. Wu, Acta Phys. Slov **47** (1997) 81.

[36] R. Scheibl, U. Heinz; nucl-th/9809092; to be submitted to Phys. Rev. C

[37] R. Mattiello, H. Sorge, H. Stöcker and W. Greiner Phys. Rev. C **53** (1997) 1443.

[38] E.M. Remler, Ann. Phys. **136** (1981) 293; M. Gyulassy, K. Frankel, and E.M. Remler, Nucl. Phys. **A402** (1983) 596; J. Aichelin, A. Rosenhauer, G. Peilert, H. Stocker, and W. Greiner, Phys. Rev. Lett. **58** (1987) 1926

[39] L. Ahle, *et al.*, Phys. Rev. **C57** (1998) R466.

FIGURES

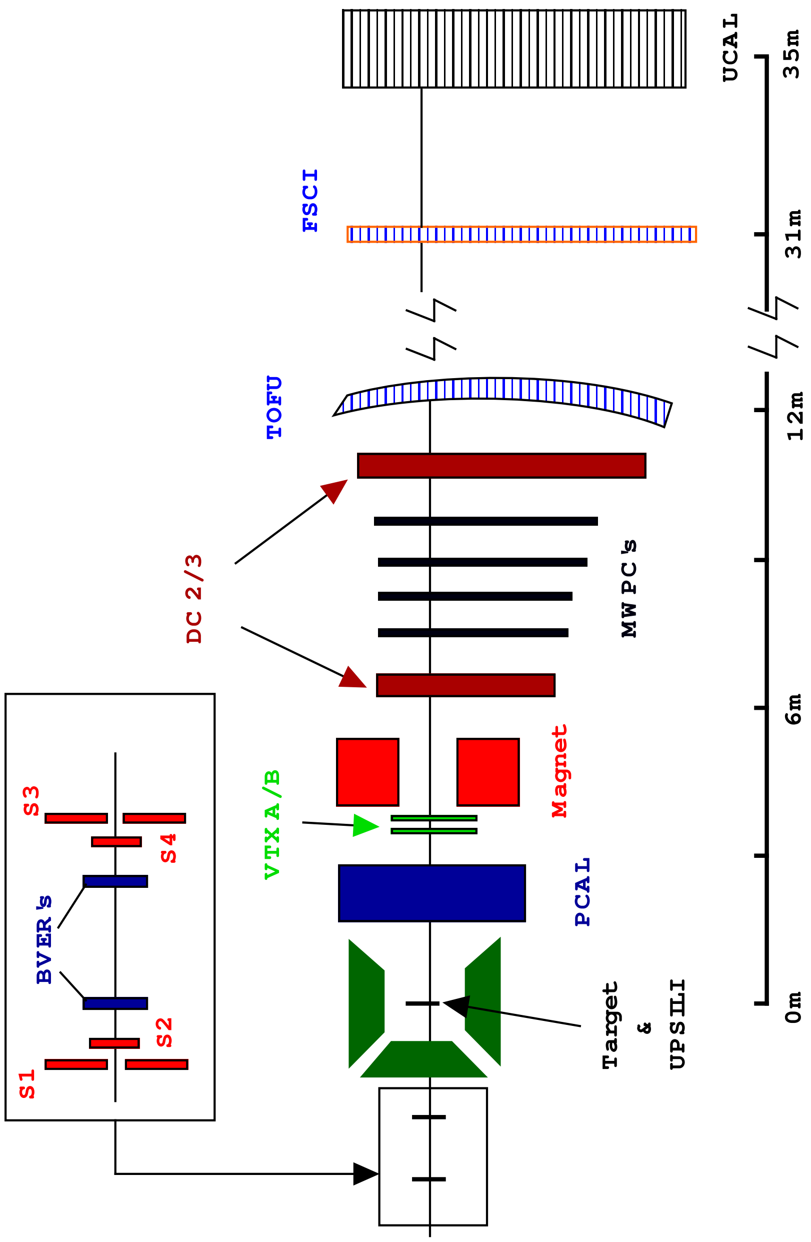

FIG. 1. E877 setup in the 1994 run

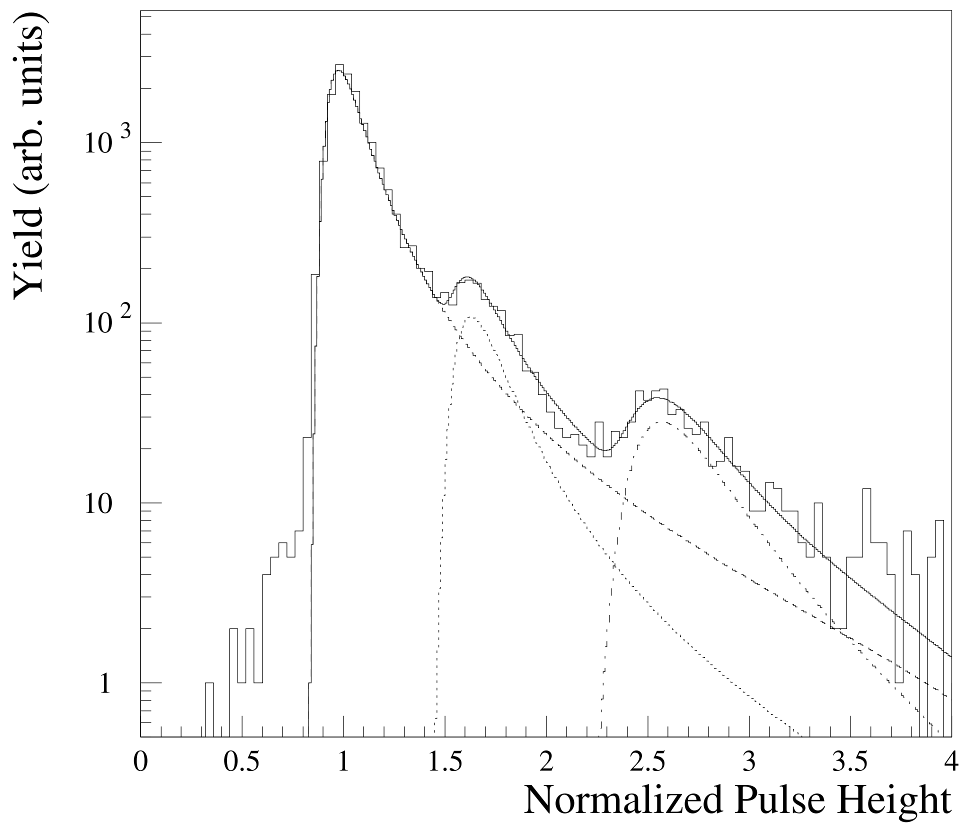

FIG. 2. A fit to the TOFU pulse height distribution for all particles at beam rapidity and from 0.5 to 1.0 GeV/c in p_t. The pulse height is normalized to the energy loss of a single $Z = 1$ minimum ionizing particle. The histogram is the measured TOFU distribution. The solid curve is the full fit while the dashed and dotted curves correspond to the individual contributions from $Z = 1$, twice $Z = 1$, and $Z = 2$ peaks.

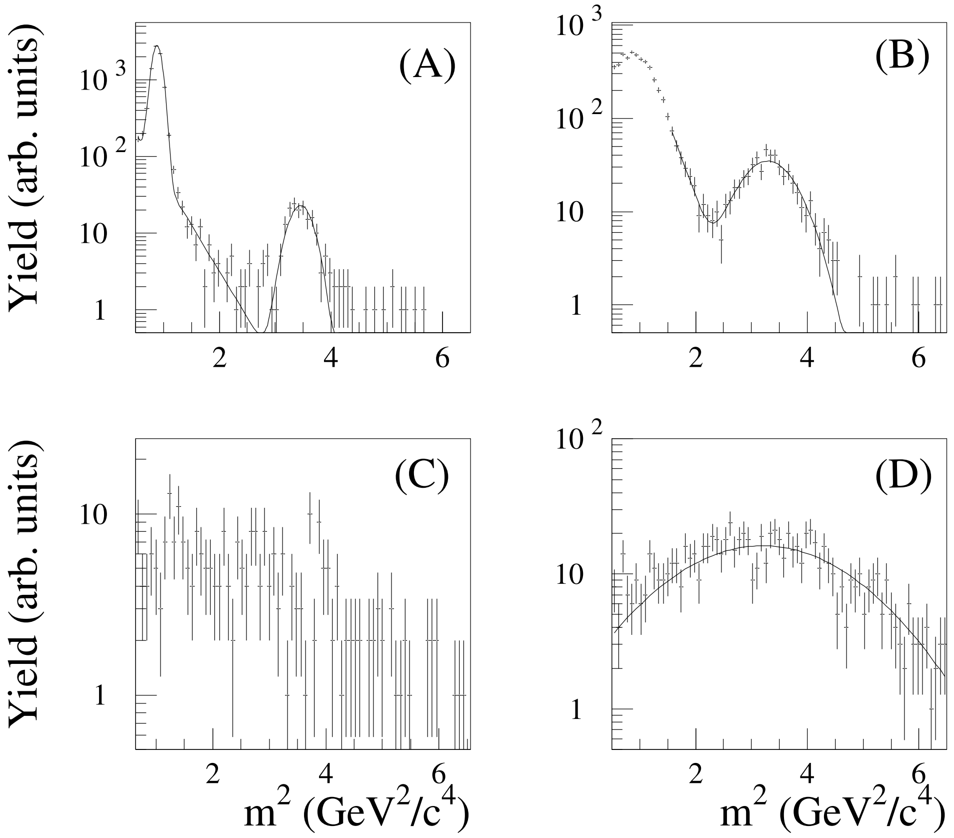

FIG. 3. Fits to the mass-squared distribution for several regions of momentum space: (A) $y = 1.4 - 1.5$, $p_t = .1 - .12$ GeV/c fit to two Gaussians and an exponential background; (B) $y = 2.2 - 2.3$, $p_t = .68 - .70$ GeV/c fit to two Gaussians; (C) $y = 2.8 - 2.9$, $p_t = .50 - .52$ GeV/c; (D) $y = 3.0 - 3.1$, $p_t = .20 - .22$ fit to a single Gaussian. See the text for details.

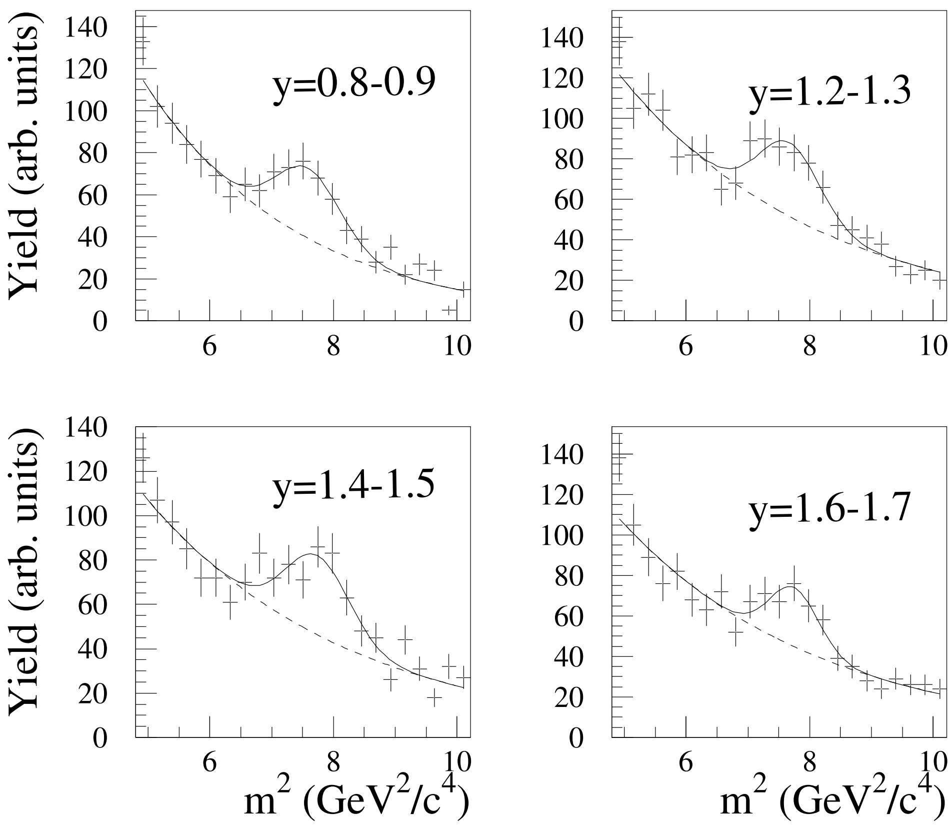

FIG. 4. Mass-squared peaks for various rapidities (calculated assuming the triton mass) fit to a Gaussian at the mass of the triton plus an exponential background from the deuteron peak.

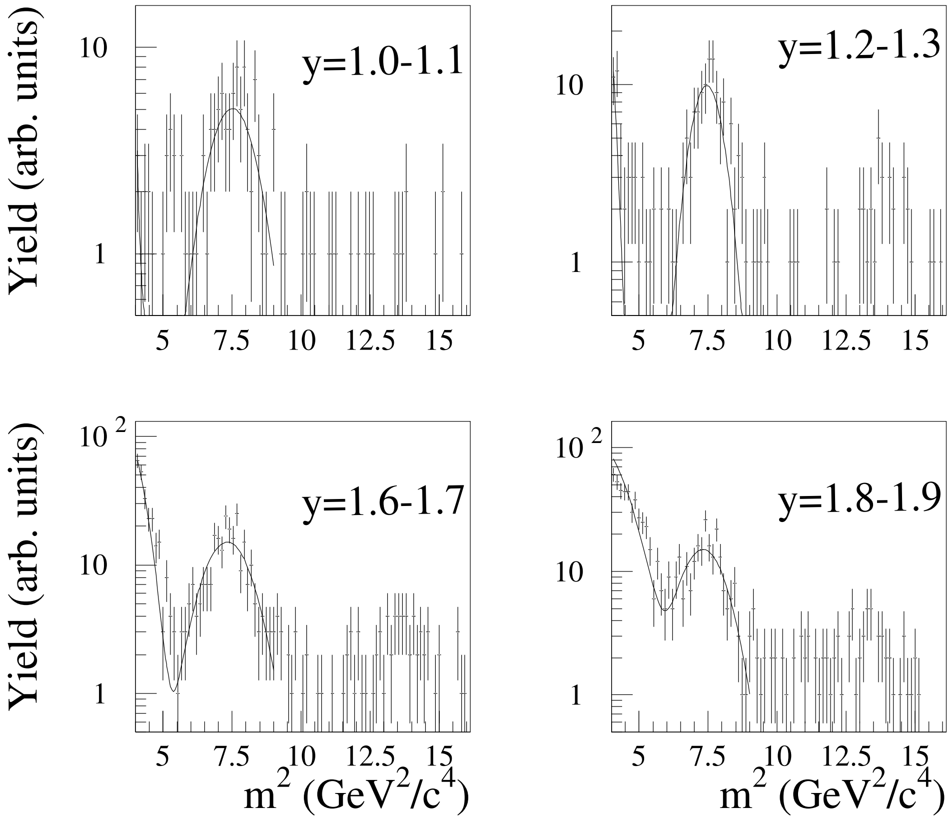

FIG. 5. Mass-squared peaks for various rapidities (calculated assuming the ^{3}He mass) and $p_t < .5$ GeV/c. A clear peak is seen at the ^{3}He mass which is lost under the proton tail for rapidities above $y \sim 2.0$.

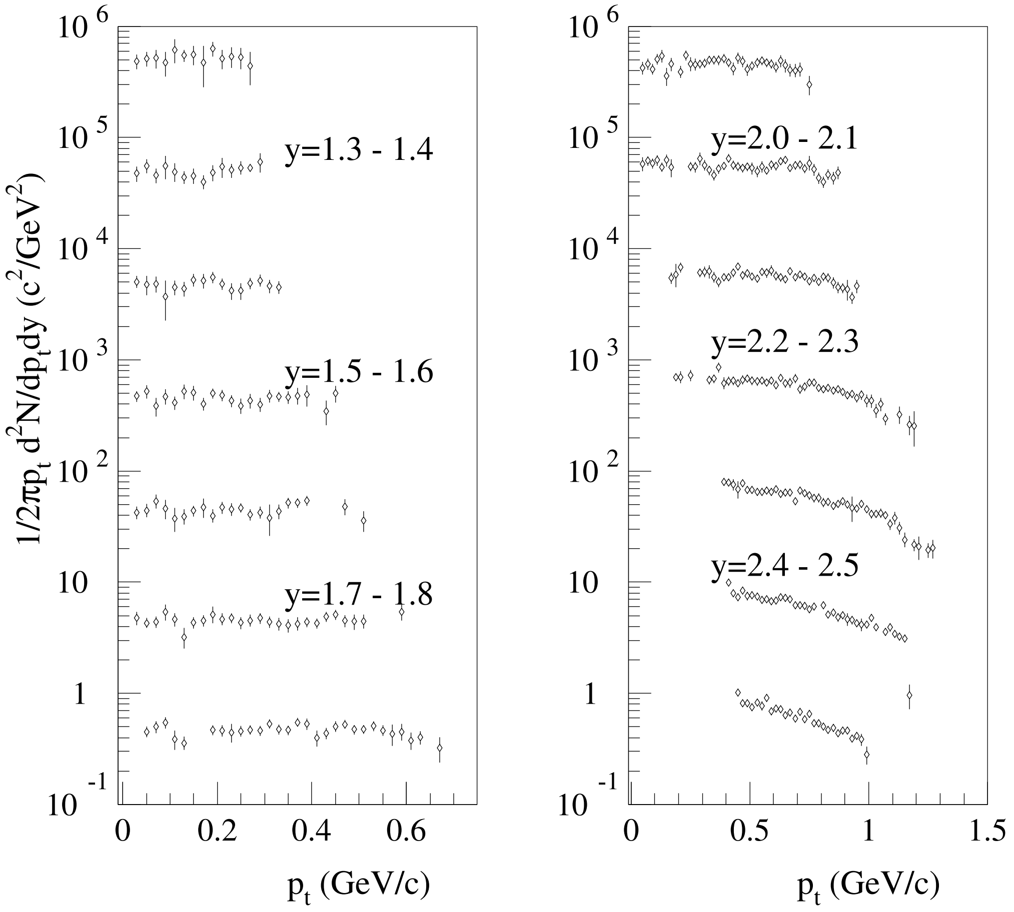

FIG. 6. Invariant multiplicities of deuterons for the 4% centrality bin. The spectra for $y = 2.5 - 2.6$ and $y = 1.8 - 1.9$ are correctly normalized and the yields for the lower rapidity bins are multiplied by successive powers of 10 for clarity of the display.

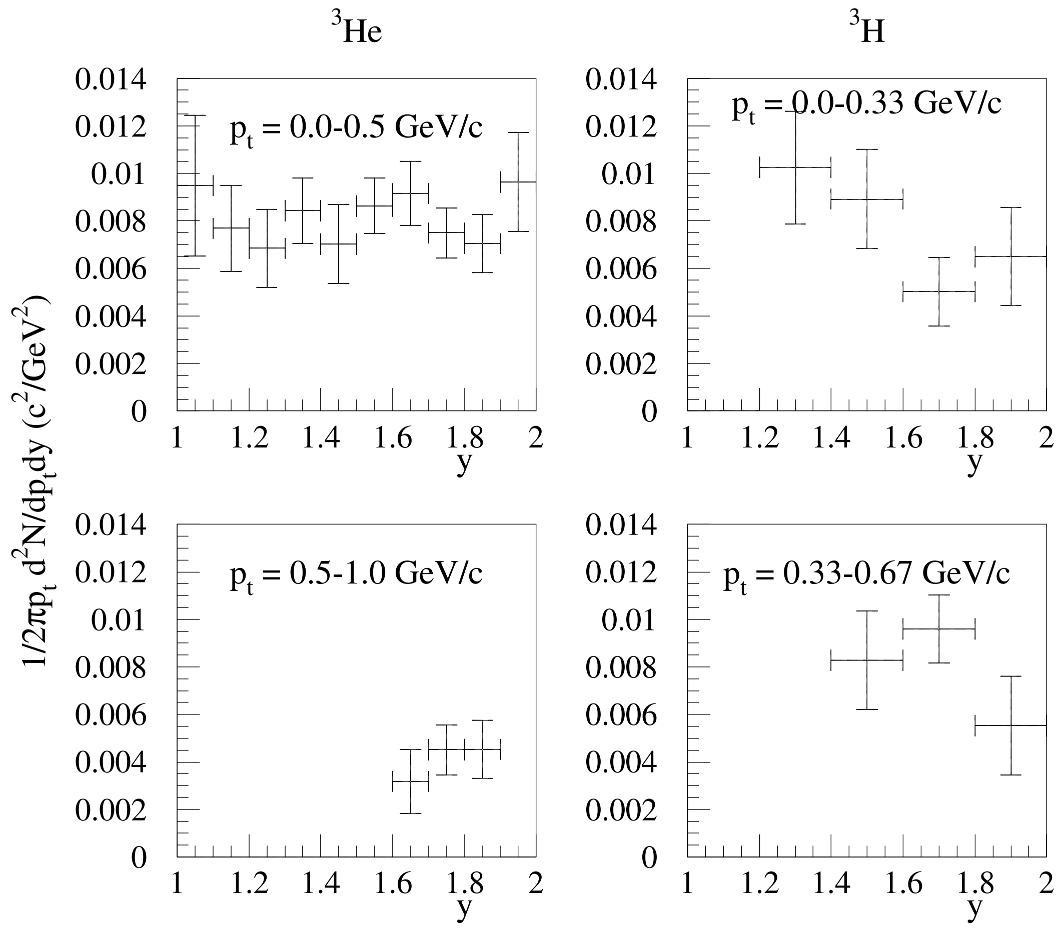

FIG. 7. Invariant multiplicities of ^{3}He and ^{3}H for the 4% inclusive centrality bin.

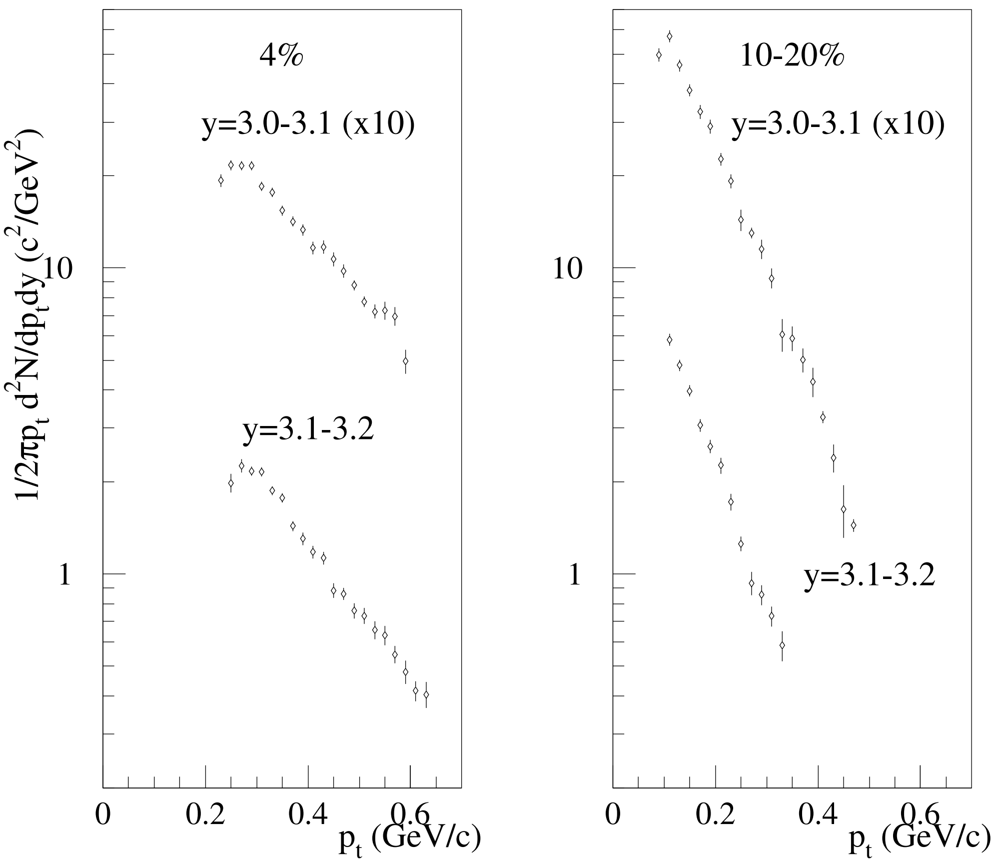

FIG. 8. Invariant multiplicities of deuterons near beam rapidity for the 4% most central collisions and the 10-20% centrality range.

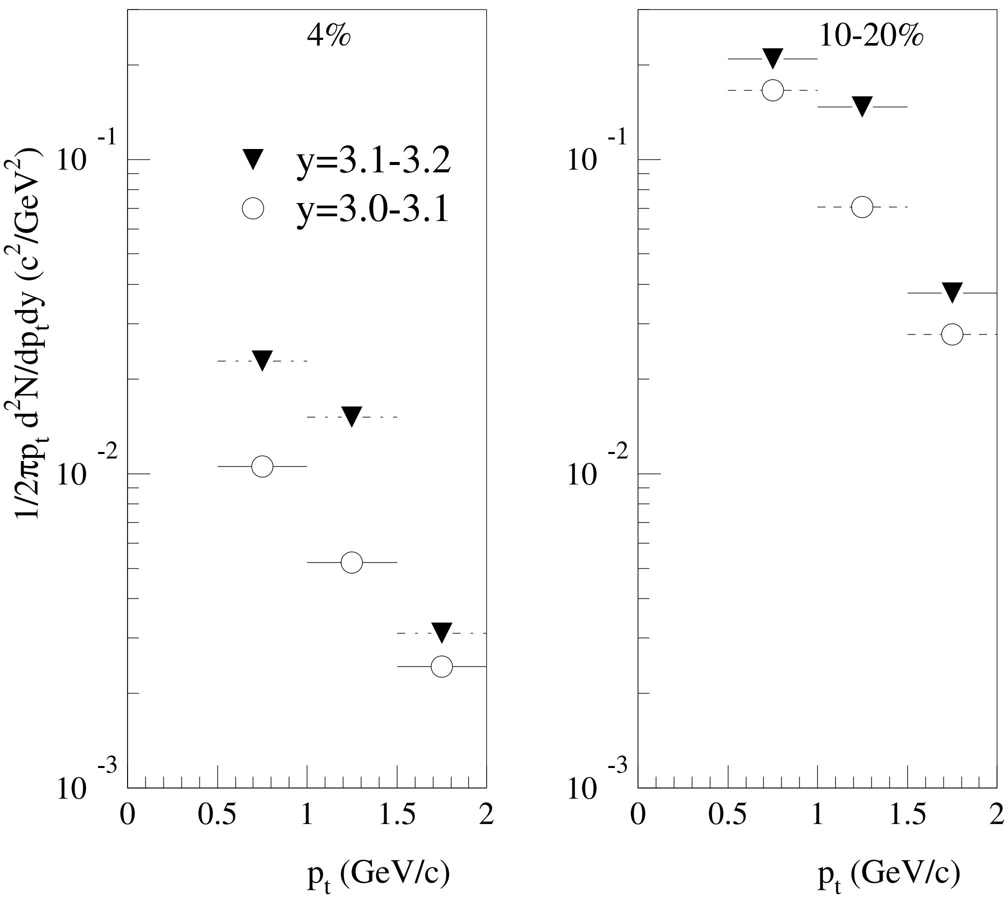

FIG. 9. ^{4}He for the 4% and 10-20% centrality bins at beam rapidity.

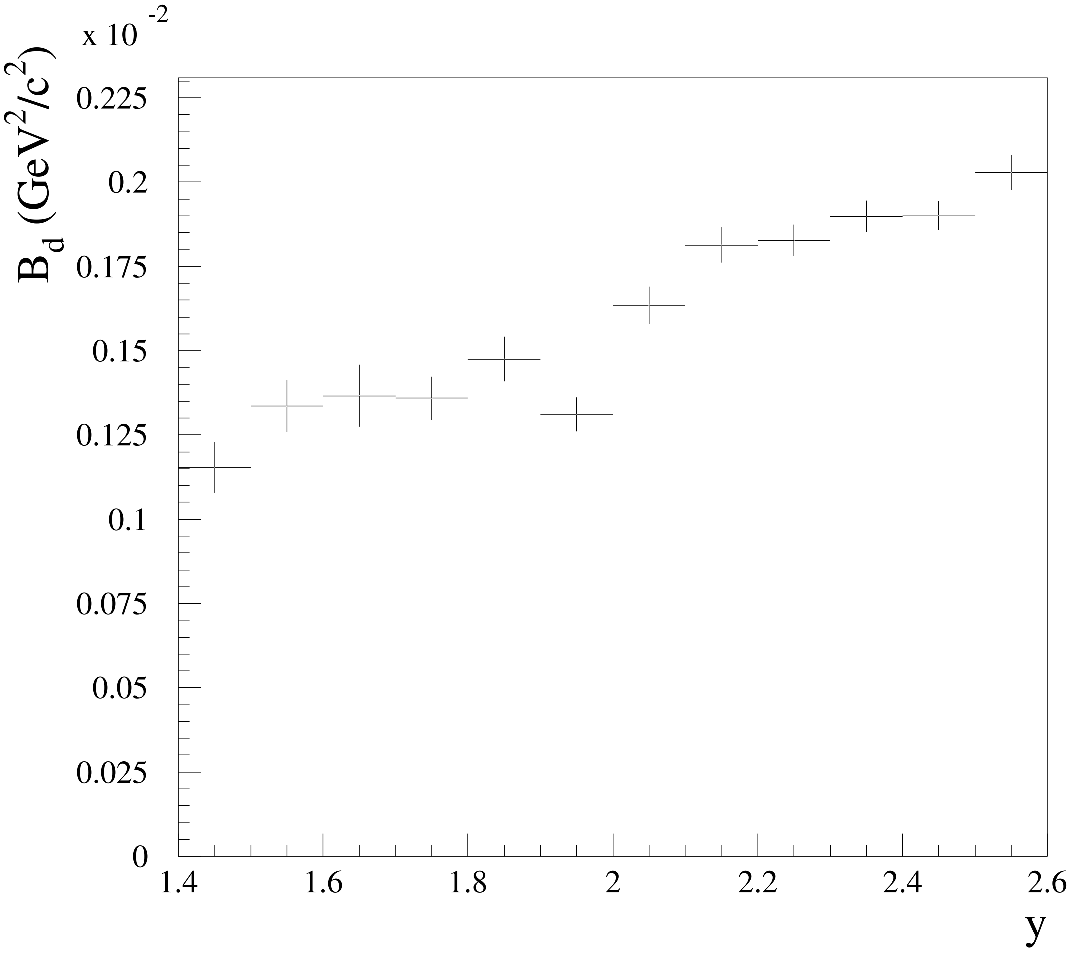

FIG. 10. B_d as a function of rapidity for the 4% most central events.

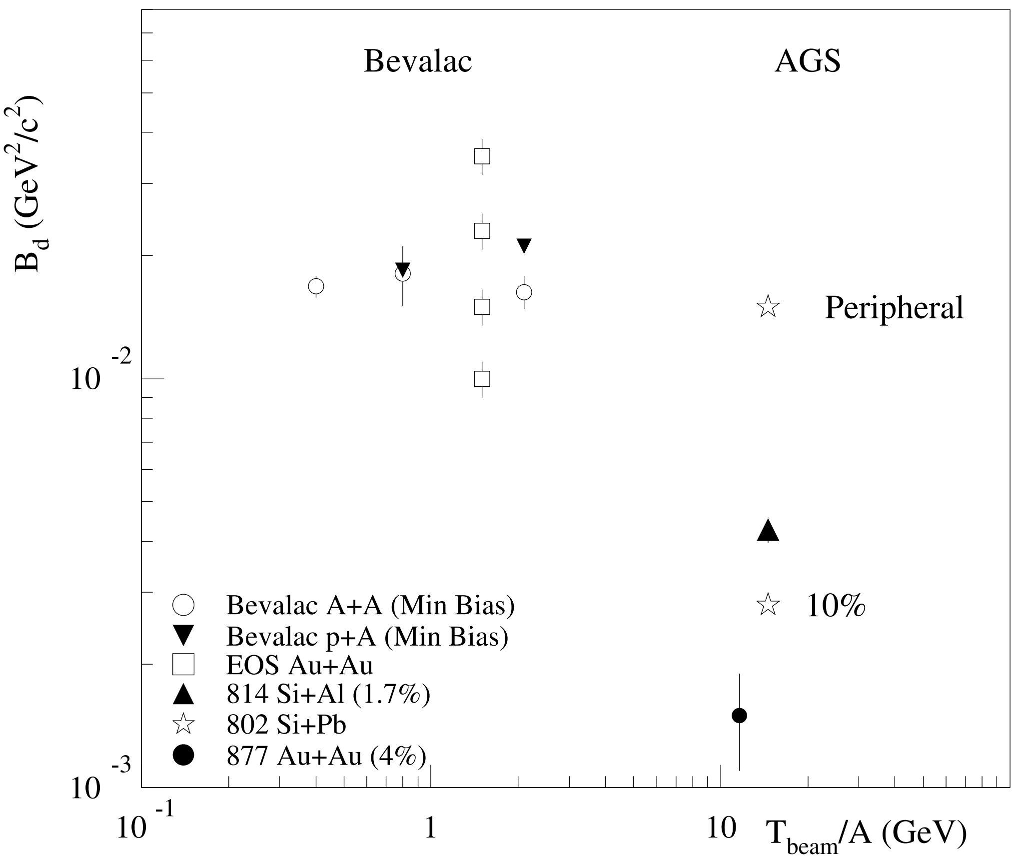

FIG. 11. B_d for a variety of systems and energies. The values in parenthesis are the centrality cut, where 'Min Bias' corresponds to minimum bias events. The Bevalac A+A data are for a variety of systems. Since no dependence on colliding system was found, the average value is shown here. The recent EOS data are measured in four seperate multiplicity bins with the highest multiplicity corresponding to the lowest value of B_d. The data are from [5,23,24,32].

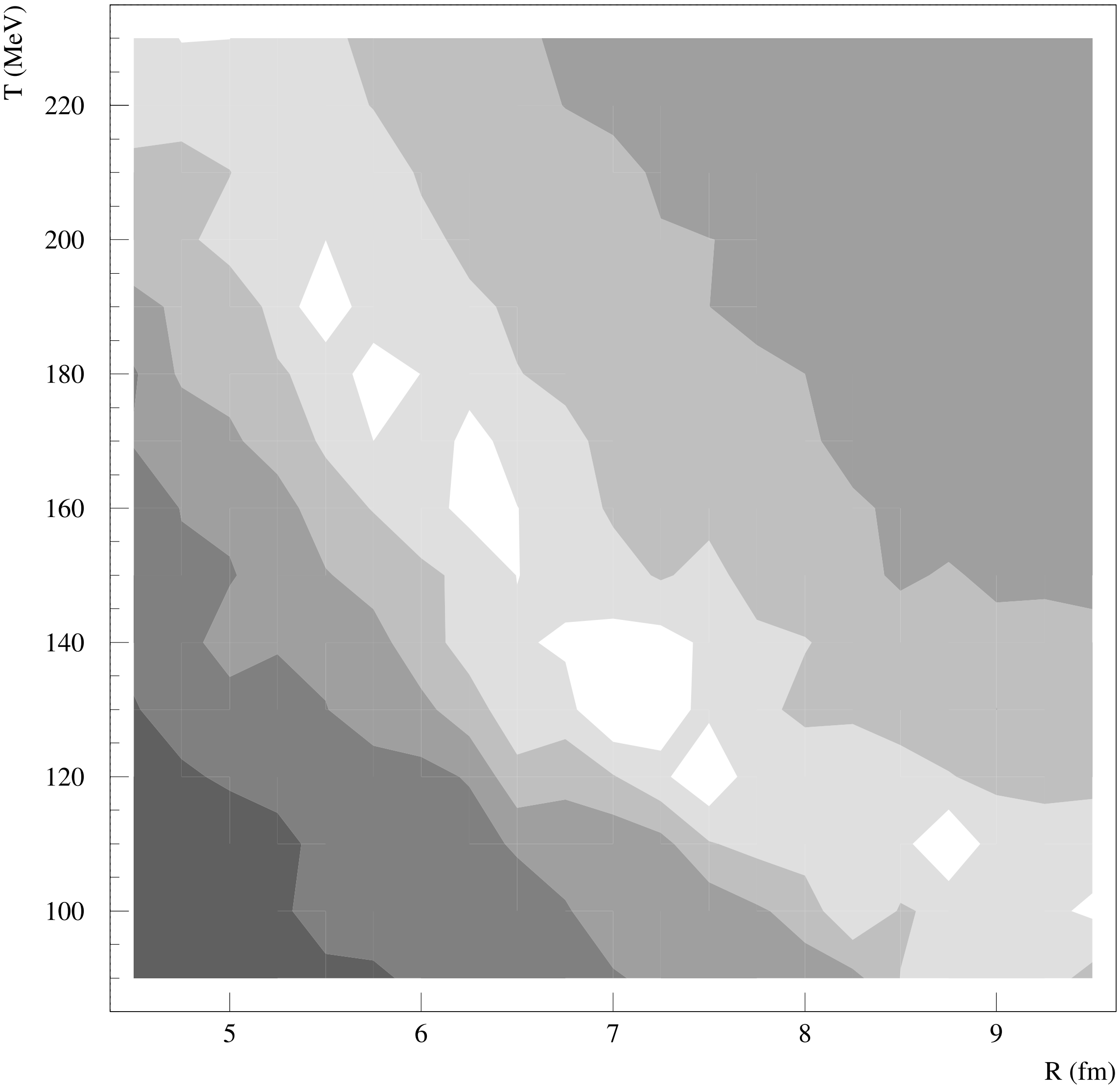

FIG. 12. χ^2 map fit to a flowing thermal model as a function of R for a variety of choices of T. Contours are located at $\chi^2 - \chi^2_{min} = 1$, 3, 10, 50, and 100 and the darker regions correspond to larger $\chi^2 - \chi^2_{min}$.